Biomedical Signal Processing and Control 75 (2022) 103552

Contents lists available at ScienceDirect

Biomedical Signal Processing and Control

journal homepage: www.elsevier.com/locate/bspc

COVID-19 CT image denoising algorithm based on adaptive threshold and optimized weighted median filter

Shuli Guo [a,1], Guowei Wang [a,1], Lina Han [b,*], Xiaowei Song [a], Wentao Yang [a]

[a] State Key Laboratory of Intelligent Control and Decision of Complex Systems, School of Automation, Beijing Institute of Technology, Beijing, China
[b] Department of Cardiology, The Second Medical Center, National Clinical Research Center for Geriatric Diseases, Chinese PLA General Hospital, Beijing, China

ARTICLE INFO

Keywords:
Median filter
COVID-19 CT image
Adaptive threshold
Weighting parameters
Hybrid genetic algorithm

ABSTRACT

CT image of COVID-19 is disturbed by impulse noise during transmission and acquisition. Aiming at the problem that the early lesions of COVID-19 are not obvious and the density is low, which is easy to confuse with noise. A median filtering algorithm based on adaptive two-stage threshold is proposed to improve the accuracy for noise detection. In the advanced stage of ground-glass lesion, the density is uneven and the boundary is unclear. It has similar gray value to the CT images of suspected COVID-19 cases such as adenovirus pneumonia and mycoplasma pneumonia (reticular shadow and strip shadow). Aiming at the problem that the traditional weighted median filter has low contrast and fuzzy boundary, an adaptive weighted median filter image denoising method based on hybrid genetic algorithm is proposed. The weighted denoising parameters can adaptively change according to the detailed information of lung lobes and ground-glass lesions, and it can adaptively match the cross and mutation probability of genetic combined with the steady-state regional population density, so as to obtain a more accurate COVID-19 denoised image with relatively few iterations. The simulation results show that the improved algorithm under different density of impulse noise is significantly better than other algorithms in peak signal-to-noise ratio (PSNR), image enhancement factor (IEF) and mean absolute error (MSE). While protecting the details of lesions, it enhances the ability of image denoising.

1. Introduction

1.1. Background & problem domain

Since December 2019, COVID-19 has spread widely around the world. According to the data released by the Johns Hopkins University, as of September 18, 2020, there were 30065728 confirmed cases in the world. The disease is highly infectious and it can cause severe acute dyspnea. Studies have shown that computed tomography (CT), as a non-invasive imaging method, is of great value in detecting lung lesions in patients with COVID-19. Therefore, CT can be used for detection and diagnosis of COVID-19. However, CT images will produce high-dose radiation in the process of acquisition, which will pose a great threat to the patient's health. Therefore, at present, the damage to the patient's body is usually reduced by decreasing the CT dose. But CT images taken with low dose usually have noise. The generation of noise will affect the quality of CT images, which will seriously affect the doctor's diagnosis for the patient's condition. Lung CT images are inevitably disturbed by various noises in the process of acquisition, transmission and storage, which will cause some random, discrete and isolated pixels on the image, that is, image noise will bring bad interference to lesion image segmentation and doctors' judgment of patients' condition.

1.2. Review of literature

At present, nucleic acid detection is the most common method to diagnose COVID-19 [1]. This method combines RNA reverse transcription and polymerase chain reaction (RT-PCR) to detect the viral RNA fragments [2,3], and the diagnosis can be confirmed by the positive nucleic acid test. However, the screening of RT-PCR has the problem of low sensitivity. Even if the RT-PCR result of suspected patient is negative, the possibility of SARS-Cov-2 infection cannot be completely ruled out [4]. In addition, nucleic acid testing has the disadvantage of time-consuming and it requires a special test kits. Therefore, it is necessary to further accelerate the detection speed and reduce the cost [5]. Through the comparative experimental analysis of CT and RT-PCR, Ai

* Corresponding author.
E-mail address: 2438381279@qq.com (L. Han).
[1] These authors contributed equally to this work.

https://doi.org/10.1016/j.bspc.2022.103552
Received 22 October 2021; Received in revised form 7 January 2022; Accepted 2 February 2022
Available online 16 February 2022
1746-8094/

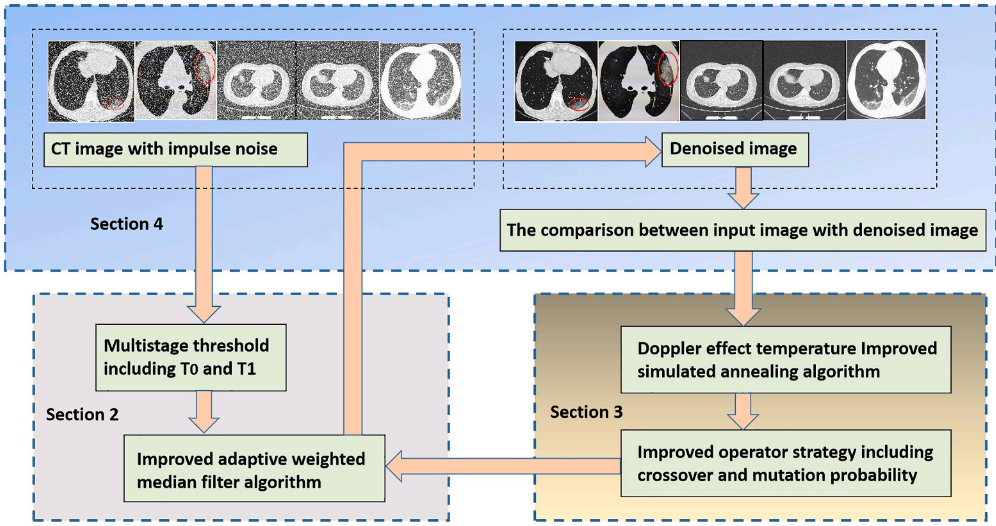

Fig. 1. Paper structure.

[6] pointed out that the diagnosis based on chest CT image is faster and more efficient than RT-PCR. Generally speaking, the lungs of patients with COVID-19 have typical imaging features [7], including ground-glass opacities (GGO), pulmonary sclerosis, pulmonary fibrosis and multiple lesions. In addition, related studies [8] have shown that the imaging information can play a vital role in the diagnosis of COVID-19. The autonomous diagnosis of COVID-19 based on artificial intelligence can minimize the contact between doctors and the virus, which reduces the chance of infection [9,10]. However, the manual analysis and diagnosis process based on CT images are highly dependent on professional knowledge [11], and the analysis of CT image features is time-consuming, which is difficult to observe hidden lesions in the early stage, and it is hard to distinguish other viral pneumonia and bacterial pneumonia [12]. The automatic diagnosis of COVID-19 can convert the visual image into the deep-level feature information [13,14], which can be quantified. It helps to reduce manual operation and improve the efficiency of accurate quantitative analysis. Standard median filter can preferably filter impulse noise. However, the traditional median filter takes the median value of the neighborhood pixels, the information points in the image may be filtered out and replaced by noise points, which will lead to the loss of some details in the image. Therefore, many scholars have proposed some improved algorithms. Verma [15] proposed adaptive median filter (AMF) algorithm, which shows good filtering performance in low-intensity noise, but when the noise density is too high, a large number of noises needs to be filtered, and the filtering window will expand. The current pixel and the replaced median may lack correlation, resulting in information loss and image blur. Sheela [16] proposed the switching median filter (SMF) method. This method determines whether each pixel is noisy. Due to the threshold needs to be defined in advance when judging the noise, the threshold remains unchanged in the processing process, the final filtering effect is not very ideal. Gupta [17] proposed a discrimination-based dual threshold median filter (DBF) method to judge whether the pixel is noisy by comparing the current pixel with the dual threshold. However, when dealing with high-intensity noise, this method is easy to produce ”tailing effect”, and the filtering performance is greatly reduced. Ahmed [18] proposed an improved discriminant-based asymmetric clipping median filter algorithm. This method can obtain good filtering effect under low-intensity noise, but under high-intensity, the filtering effect is very poor and some details are lost. There are some state-of-the-art methods about denoising algorithm reported. Zhao [19] obtains the residual spectrum according to logarithmic amplitude spectrum of the image, and then the inverse Fourier transform is used to obtain the saliency map. Although this method can suppress the image noise, the subtraction operation is used in the process of calculating the log amplitude. It not only suppresses the noise, but also restrains the detail information, which is not conducive to the denoising of the COVID-19 image. The CNN denoising method [20] can effectively use the global features of the image to significantly improve the denoising effect. The lower the number of CNN layers, the more primitive the extracted low-level features, such as color and edge lines. However, with the deepening of the network, the features extracted by the CNN method become more advanced, and a large number of low-level features will be lost. Yan [21] proposed a KSVD image denoising algorithm based on K-means and singular value decomposition (SVD). This method is based on the bayesian reconstruction theory, and it uses the K-means clustering to obtain an optimal signal sparse representation dictionary set. Through the linear combination of the dictionary elements, various signals are constructed to remove the noise in the CT image. However, dictionary learning brings high computational cost, resulting in too long time for image denoising. In addition, the KSVD method is also insufficient for denoising of high-proportion noisy images. Yahya [22] proposed block-matching and 3D filtering (BM3D) algorithm, which has achieved good results in various image denoising processes, but it is easy to cause tissue contour blur when denoising low-dose CT image. Moreover, there are a lot of parameters in the BM3D algorithm that need to be set manually, which severely limits the effect of the practical application. Gu [23] proposed a weighted kernel norm minimization (WNNM) denoising algorithm. This method can characterize the difference of image effect according to the matrix singular value, given different weights, and it highlights the important information for the image. However, this algorithm needs time-consuming SVD calculation and iterative approximation, which is slow and inefficient.

1.3. *Gaps identified from review*

The above improved algorithms have great improvements in filtering performance, but there are still some deficiencies in dealing with image detail blur. The lesions of COVID-19 mainly show various forms of ground-glass or consolidation shadow. In the early imaging of COVID-19, the change of lesions is not obvious, and the density is low, which is easy to confuse the early lesions of COVID-19 with noise. On the other hand, the lesions of ground-glass in the advanced stage are uneven and it have similar gray values to the CT images of suspected COVID-19 cases such as adenovirus pneumonia and mycoplasma pneumonia. The traditional weighted median filter denoising algorithm has the problems of low contrast and fuzzy boundary.

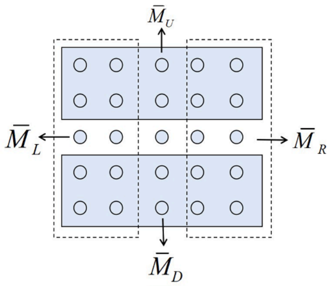

$$\begin{bmatrix} f(i\text{-}2,j+2) & f(i\text{-}1,j+2) & f(i,j+2) & f(i+1,j+2) & f(i+2,j+2) \\ f(i\text{-}2,j+1) & f(i\text{-}1,j+1) & f(i,j+1) & f(i+1,j+1) & f(i+2,j+1) \\ f(i\text{-}2,j) & f(i\text{-}1,j) & f(i,j) & f(i+1,j) & f(i+2,j) \\ f(i\text{-}2,j-1) & f(i\text{-}1,j-1) & f(i,j-1) & f(i+1,j-1) & f(i+2,j-1) \\ f(i\text{-}2,j-2) & f(i\text{-}1,j-2) & f(i,j-2) & f(i+1,j-2) & f(i+2,j-2) \end{bmatrix}$$

Fig. 2. Filter window and gray value.

1.4. Highlights

The highlights of this work can be summarized as the following: (i) the adaptive two-stage threshold method is proposed, which reduces the misjudgment of noise signal points and improves the accuracy of detection for COVID-19; (ii) we develop the weighted median filter image denoising method based on adaptive hybrid genetic. The weighted denoising parameters can adaptively change according to the detailed information of lung lobes and ground-glass lesions, it can enhance the ability of image denoising while better protecting the details of the lesions; (iii) the cross and mutation probability of genetic algorithm based on the steady-state regional population density is advanced, which obtains a more accurate COVID-19 denoised image with relatively few iterations; (iv) in order to reduces the CPU time and improve the efficiency of the optimal solution, we investigate the doppler effect temperature improved simulated annealing algorithm.

1.5. Paper structure

The rest of this paper is organized as follows. Section 2 describes the multi-level threshold algorithm and its mathematical properties, and we present the algorithm of adaptive center weighted median filtering. In Section 3, we propose the adaptive hybrid genetic method and the advanced simulated annealing algorithm according to these properties. In Section 4, we show the simulation experiments for the different kinds of COVID-19 CT images. The paper is structured as shown in Fig.1.

2. Multi-level threshold center weighted adaptive median filtering algorithm

The CT image of early COVID-19 is easily confused by noise. The traditional extreme noise points judgment [24–27] can easily cause misdiagnosis of COVID-19 lesion signals. For the single threshold filtering method, the pixel whose value exceeds the preset threshold will be judged as noise [28–30]. Therefore, using a single threshold method may increase the probability of error detection for noise. Hence, a median filtering method based on adaptive multi threshold discrimination is proposed. In this method, the noise pixels will be discriminated in a relatively narrow interval. Thus, this will improve the accuracy of noise detection.

2.1. Multi-level threshold calculation method

Calculation of threshold T_0: this threshold is the first step of noise point detection. The purpose is to find suspected noise points. It can calculate the gray value of each pixel, the median gray value of the filter window, the gray average value of the four rectangular neighborhood windows on the top, bottom, left and right of the point (i, j). The calculation of threshold T_0 is:

$$\begin{aligned} T_0 = & \frac{1}{n}\left|\sum_{m=-2}^{2}\sum_{n=-2}^{2}\left[f\left(i+m,j+n\right)-f_{med}\right]\right|^{\frac{1}{2}}+ \\ & \frac{1}{n}\left|\sum_{m=-2}^{2}\sum_{n=-2}^{2}\left[f\left(i+m,j+n\right)-f_{ave}\right]\right|^{\frac{1}{2}}+ \\ & \frac{1}{n}\left|\sum_{m=-2}^{2}\sum_{n=-2}^{2}\left[f\left(i+m,j+n\right)-\overline{M}_U\right]\right|^{\frac{1}{2}}+ \\ & \frac{1}{n}\left|\sum_{m=-2}^{2}\sum_{n=-2}^{2}\left[f\left(i+m,j+n\right)-\overline{M}_D\right]\right|^{\frac{1}{2}}+ \\ & \frac{1}{n}\left|\sum_{m=-2}^{2}\sum_{n=-2}^{2}\left[f\left(i+m,j+n\right)-\overline{M}_L\right]\right|^{\frac{1}{2}}+ \\ & \frac{1}{n}\left|\sum_{m=-2}^{2}\sum_{n=-2}^{2}\left[f\left(i+m,j+n\right)-\overline{M}_R\right]\right|^{\frac{1}{2}} \end{aligned} \quad (1)$$

The variable n and m represent the length and the width of the filter window respectively(the length and width are equal), and f(i,j) represents the gray value of the current pixel. f_{med} is the median gray value of all pixels in the filter window, and f_{ave} is the average gray value of all pixels in the filter window. Four neighborhood rectangular windows of 5×2 and 2×5 are defined on the top, bottom, left and right directions of the point (i,j), and the gray average values corresponding to the four neighborhood windows are defined as $\overline{M}_U, \overline{M}_D, \overline{M}_L$ and $\overline{M}_R$, as shown in

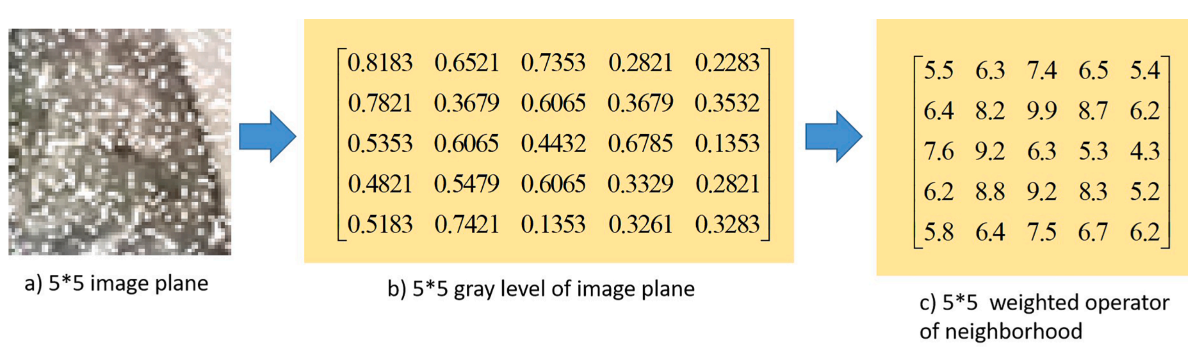

Fig. 3. Weighting operator based on 5 * 5 image plane.

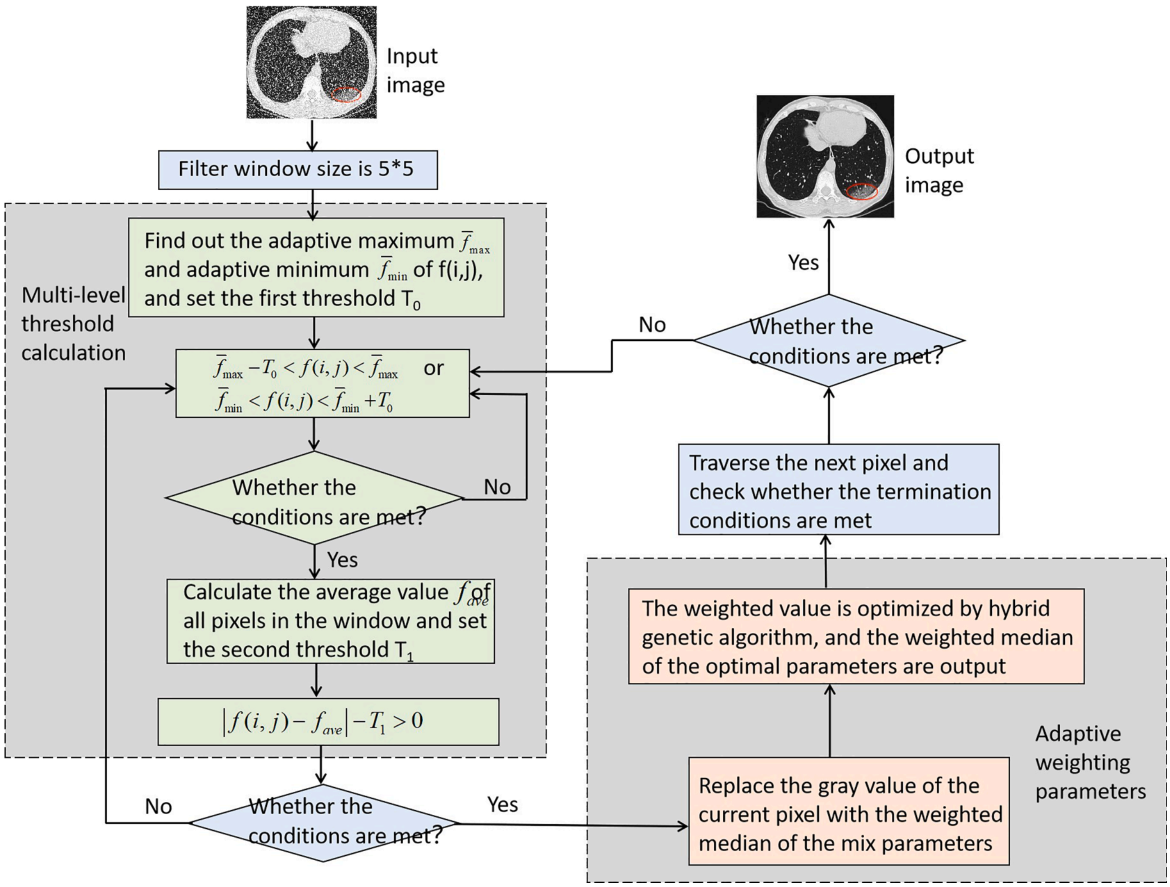

Fig. 4. Flow chart of median filtering based on adaptive threshold and optimized weighting parameters.

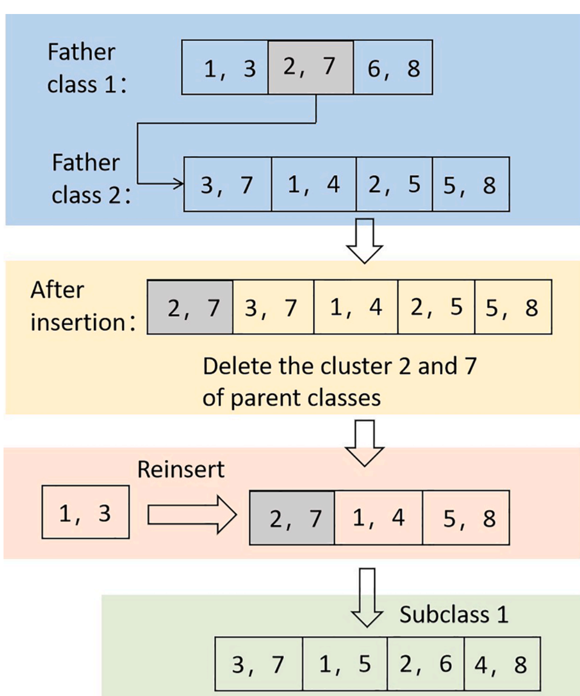

Fig. 5. Adaptive hybrid cross operation.

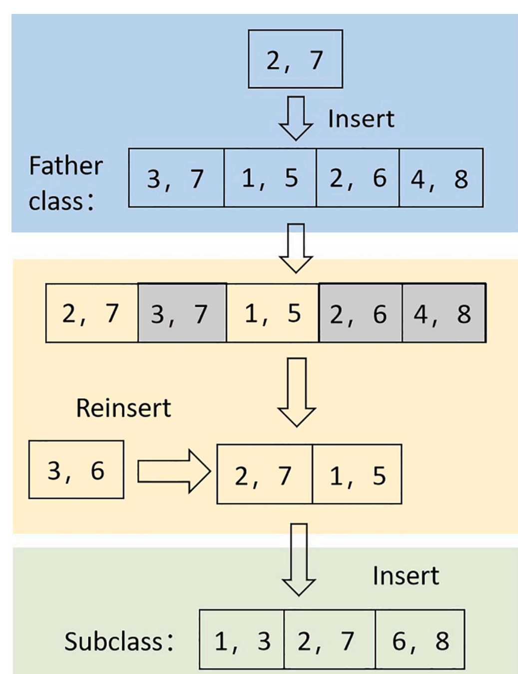

Fig. 6. Adaptive hybrid mutation operation.

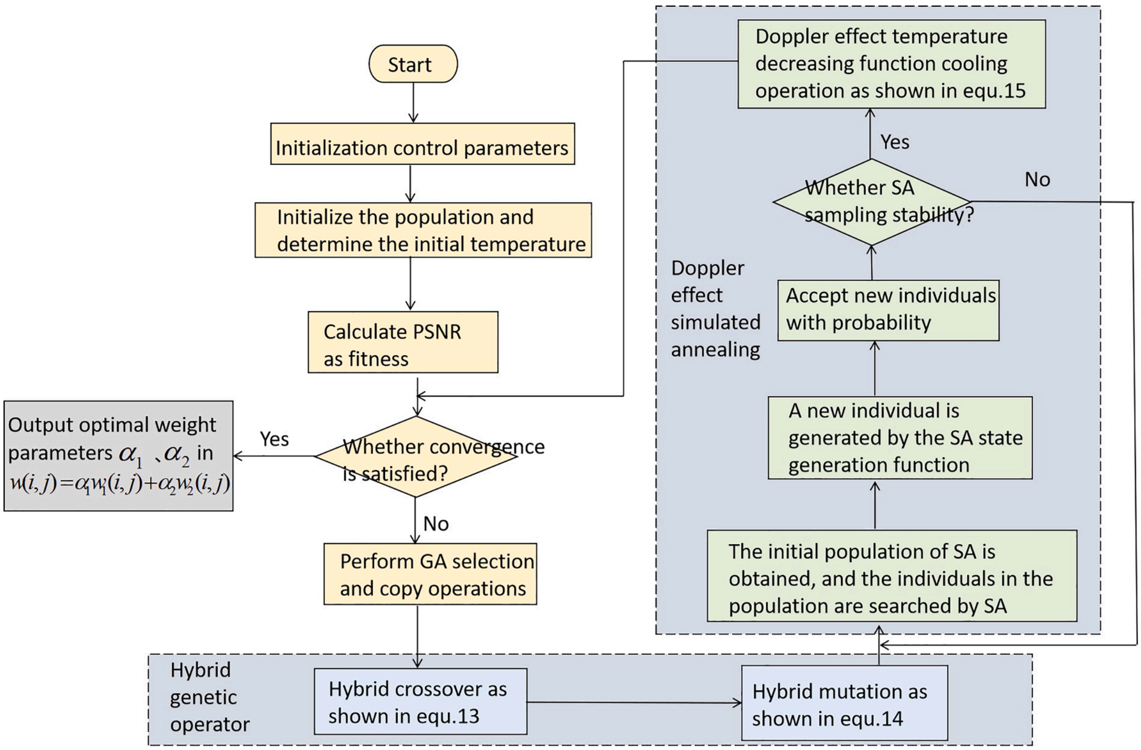

Fig. 7. Flow chart of adaptive genetic operator strategy.

Fig.2. The value calculation formula is:

$$\overline{M}_U = \frac{\sum_{k=-2}^{-1}\sum_{l=-2}^{2} f\left(i+k, j+l\right)}{5 \times 2} \tag{2}$$

$$\overline{M}_D = \frac{\sum_{k=-2}^{2}\sum_{l=-2}^{-1} f\left(i+k, j+l\right)}{5 \times 2} \tag{3}$$

$$\overline{M}_L = \frac{\sum_{k=1}^{2}\sum_{l=-2}^{2} f\left(i+k, j+l\right)}{5 \times 2} \tag{4}$$

$$\overline{M}_L = \frac{\sum_{k=-2}^{2}\sum_{l=1}^{2} f\left(i+k, j+l\right)}{5 \times 2} \tag{5}$$

Calculation of the second threshold T_1: this threshold is the second step for noise point detection. When the point is determined to be a suspected noise point, the average gray value of all pixels in the filter window is calculated. If the gray value of the point is significantly different from the average value, it can be determined that the current point is a noise point and needs to be replaced by the median value. Through the further accurate judgment for the suspected noise point by the second threshold T_1, the calculation of T_1 is:

$$T_1 = \varphi p = \left(F_1 + F_2\right) \times \frac{N_{pn}}{n \times n} \tag{6}$$

The variable φ is the regulatory factor of threshold T_1, $\varphi = F_1 + F_2$, the expression of f_1 and f_2 is:

$$F_1 = \frac{n}{n}\left|\sum_{k=-2}^{2}\sum_{l=-2}^{2}\left[f\left(i+k, j+l\right) - f_{med}\right]\right| \tag{7}$$

$$F_2 = \frac{n}{n}\left|\sum_{k=-2}^{2}\sum_{l=-2}^{2}\left[f\left(i+k, j+l\right) - F_1\right]\right| \tag{8}$$

p is the image noise density, the expression is $p = \frac{N_{pn}}{n\times n}$; N_{pn} represents the number of noise points in the window. The threshold T_1 increases with the increase of noise density, and the threshold value is related to the noise density, so as to realize the adaptive selection of the threshold in the same image under different noise density.

2.2. Adaptive weighted median filter algorithm

The lesions of ground-glass in the advanced COVID-19 show non-uniformity, which is similar to the CT images of COVID-19 suspected cases such as adenovirus pneumonia and mycoplasma pneumonia. Aiming at the problems of low contrast and fuzzy boundary in the traditional median filter denoising algorithm, a weighted median filter image denoising method based on adaptive hybrid genetic algorithm is proposed, so that the weighted denoising parameters can adapt to the changes according to the details of lung lobes and ground-glass lesions. Based on the steady-state regional population density, the cross and the mutation probability of genetic is adaptively matched to obtain a more accurate denoised CT image of COVID-19 with relatively few iterations. The calculation of the center weighted filtering [31–34] is:

$$f(i,j)_{CWM} = median\left\{w\left(i,j\right) \times f\left(i,j\right), f\left(r,s\right) \middle| f\left(r,s\right) \in N^{o}_{p(i,j)}\right\} \tag{9}$$

$w(i,j) \times f(i,j)$ represents the gray value when the weight of f(i,j) is w(i,j), $f(i,j)_{CWM}$ is the center weighted median gray value, f(i,j) represents the gray value of pixel p(i,j), $N^{o}_{p(i,j)}$ represents the hollow neighborhood of pixel p(i,j), and f(r,s) represents the gray value corresponding to all pixels in $N^{o}_{p(i,j)}$. The improved weight of the center weighted filtering is:

$$w(i,j) = \alpha_1 w_1(i,j) + \alpha_2 w_2(i,j) \tag{10}$$

α_1 and α_2 are weight parameters, which is optimized by the adaptive

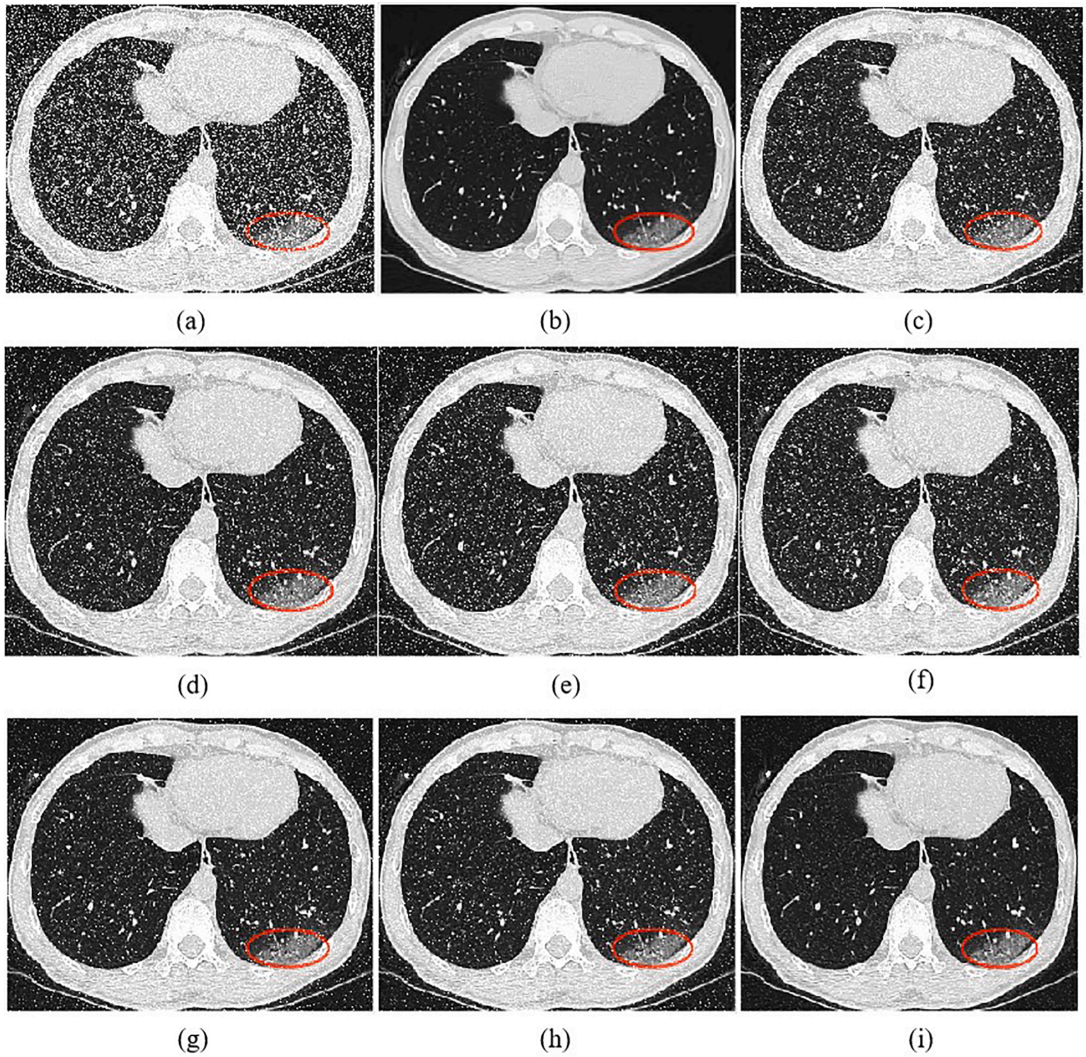

Fig. 8. CT image of early COVID-19 (a) impulse (40%) noise; (b) original CT image; (c) denoised image by TDMF; (d) denoised image by MMF; (e) denoised image by SMF; (f) denoised image by DBACMF; (g) denoised image by CWMF; (h) denoised image by AMF; (i) denoised image by TWMF.

Table 1
Comparison of TWMF with different methods for CT image of early COVID-19.

Denoising method	MSE/ dB	PSNR/ dB	IEF
TDMF	288.5	23.5	129.4
MMF	256.3	24.0	131.6
SMF	166.7	26.3	135.6
DBACMF	154.6	26.8	139.5
CWMF	130.3	27.0	142.7
AMF	112.8	27.6	145.4
TWMF	**81.6**	**29.0**	**173.7**

hybrid genetic algorithm. The weighted sub coefficient $w_1(i,j)$ is set in the weighted coefficient w(i,j), $w_1(i,j)$ is used to characterize the similarity between the current pixel and the median pixel f_{med}(representing uncontaminated point). The smaller the similarity value, the greater the correlation. The calculation of the weighted sub coefficient $w_1(i,j)$ is:

$$w_1\left(i,j\right) = \frac{\frac{1}{1+max\left\{T_{mean},(f(i-r,j-r)-f_{med})^2\right\}}}{\sum_{(i-r,j-r)\in W_r}\frac{1}{1+max\left\{T_{mean},(f(i-r,j-r)-f_{med})^2\right\}}} \tag{11}$$

T_{mean} represents the average value for the square of the difference between each pixel value and its average value, which is calculated as following:

$$T_{mean} = \frac{\sum_{(i-r,j-r)\in W_r}(f(i-r,j-r)-f_{mean})^2}{N_r} \tag{12}$$

N_r is the total number of window pixels and f_{mean} is the average value of all pixels in the current window. A weighted sub coefficient $w_2(i,j)$ is set in the weighted coefficient w(i,j), and $w_2(i,j)$ is used to characterize the similarity between the current pixel and the nearest noise point. According to the pixel space distance value, a distance correlation function Q(i,j) is designed to characterize the correlation between the current pixel and the noise points. The weighted coefficient $w_2(i,j)$ should meet the following conditions:① $w_2(i,j)$ is a non-decreasing function with Q(i, j), that is, the greater the Q(i,j), the greater the weight value to be added;② $w_2(i,j)$When Q(i,j) is small, w(i,j) should increase slightly, and when Q(i,j) is large, w(i,j) should increase greatly, that is, w(i,j) is positively correlated with Q(i,j). Setting the current pixel as f(i,j), and f (s,t) is the noise point pixel nearest to the current pixel. Combined with the weighted distance and its normalization, the following weighted function is obtained, which meets positive correlation and the requirement of human vision. Setting the weighted function is:

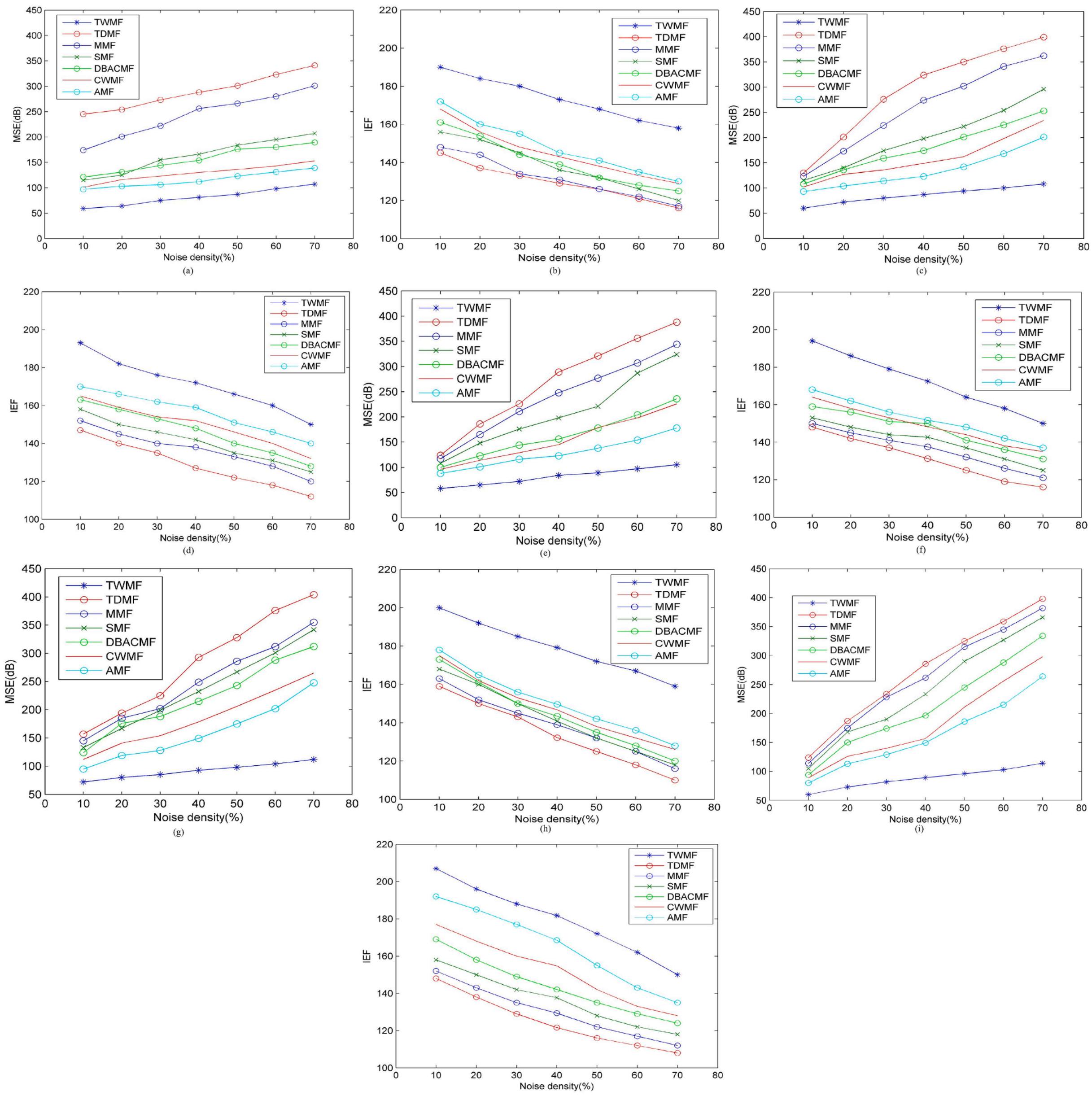

Fig. 13. Early COVID-19 with different noise density: (a) comparison of the MSE; (b) comparison of the IEF. Advanced COVID-19 with different noise density: (a) comparison of the MSE; (b) comparison of the IEF. Adenovirus pneumonia with different noise density: (a) comparison of the MSE; (b) comparison of the IEF. Early COVID-19 with non-symptom by different noise density: (a) comparison of the MSE; (b) comparison of the IEF. Advanced COVID-19 with non-symptom by different noise density: (a) comparison of the MSE; (b) comparison of the IEF. .

Table 6
Comparison of TWMF with different methods for CT image of early COVID-19 with different noise density.

Noise	Index	**TWMF**	TDMF	MMF	SMF	DBACMF	CWMF	AMF
10%	MSE/IEF	**59.3/190.5**	245.7/145.5	174.8/148.6	115.3/156.7	121.6/161.8	101.8/168.6	97.6/172.4
20%	MSE/IEF	**64.6/184.4**	254.9/137.1	201.3/144.8	125.1/152.8	131.9/154.1	116.2/156.8	103.7/160.8
30%	MSE/IEF	**75.3/180.7**	273.7/133.8	222.9/134.1	155.6/145.8	144.9/144.6	123.5/148.4	106.9/155.5
40%	MSE/IEF	**81.6/173.7**	288.5/129.4	256.3/131.6	166.7/135.6	154.6/139.5	130.3/142.7	112.8/145.4
50%	MSE/IEF	**87.6/168.3**	301.4/126.8	266.7/126.5	184.9/132.4	176.2/132.7	136.7/138.8	123.2/141.6
60%	MSE/IEF	**98.9/162.6**	323.9/121.2	280.7/122.2	195.9/126.5	180.7/128.5	143.2/133.5	131.4/135.8
70%	MSE/IEF	**107.2/158.7**	341.9/116.3	301.8/117.6	207.2/120.5	189.2/125.7	153.6/129.2	139.3/130.7

$$w_2\left(i,j\right) = 1 - \frac{c}{\left(1 + e^{\frac{1}{Q(i,j)}}\right)\sum_{i=1}^{n}\frac{1}{Q(i,j)}\left(n\times n\right)} \tag{13}$$

$$Q\left(i,j\right) = \frac{\sqrt{(s-i)^2 + (t-j)^2}}{n} \tag{14}$$

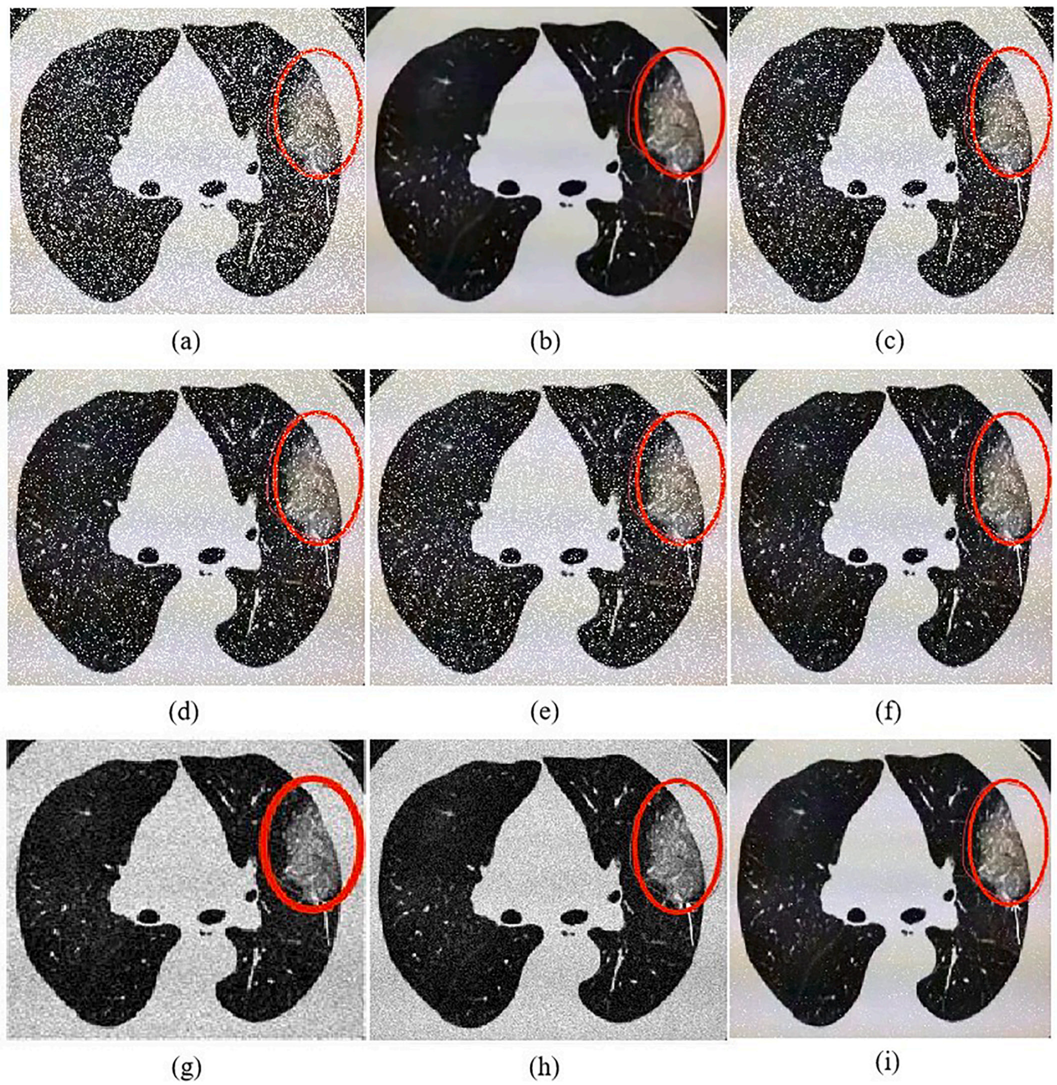

Fig. 9. CT image of advanced COVID-19 (a) impulse (40%) noise; (b) original CT image; (c) denoised image by TDMF; (d) denoised image by MMF; (e) denoised image by SMF; (f) denoised image by DBACMF; (g) denoised image by CWMF; (h) denoised image by AMF; (i) denoised image by TWMF.

Table 2
Comparison of TWMF with different methods for CT image of advanced COVID-19

Denoising method	MSE/dB	PSNR/dB	IEF
TDMF	324.4	23.0	127.1
MMF	274.7	23.7	138.0
SMF	198.7	25.2	142.9
DBACMF	174.8	25.7	148.5
CWMF	149.4	26.4	152.8
AMF	123.7	27.2	159.5
TWMF	**87.1**	**28.7**	**172.4**

Where, c is the distance constant, which is related to the size of the filter window, $c = \frac{1}{(n\times n+1)/2}$. Therefore, the c value of 5x5 detection window used in this paper is $c = \frac{1}{(5\times 5+1)/2} = \frac{1}{13}$.Through the optimal combination for (α_1, α_2), the relatively optimal denoising effect in the spatial domain can be obtained. The pixel weighted coefficient is represented as shown in Fig.3.

2.3. Improvement steps

Step 1: find out the maximum gray value $\overline{f}_{max}$ and minimum gray value $\overline{f}_{min}$ in the filter window, which is compared with the current pixel

Table 7
Comparison of TWMF with different methods for CT image of advanced COVID-19 with different noise density

Noise	Index	TWMF	TDMF	MMF	SMF	DBACMF	CWMF	AMF
10%	MSE/IEF	**60.1/193.3**	130.5/147.7	123.5/152.6	115.3/158.6	108.5/163.3	102.2/165.6	93.5/170.3
20%	MSE/IEF	**72.5/182.5**	201.7/140.7	173.4/145.8	140.4/150.8	136.7/158.2	127.3/159.9	104.8/166.3
30%	MSE/IEF	**80.7/176.5**	276.3/135.6	224.3/140.6	174.3/146.9	159.9/153.2	136.3/154.2	114.2/162.9
40%	MSE/IEF	**87.1/172.4**	324.4/127.1	274.7/138.0	198.7/142.9	174.8/148.5	149.4/152.8	123.7/159.5
50%	MSE/IEF	**94.4/166.7**	350.7/122.5	302.8/133.3	222.3/135.5	201.9/140.3	162.4/146.7	142.5/151.9
60%	MSE/IEF	**100.5/160.8**	376.8/118.8	341.2/128.9	254.3/131.8	225.5/135.7	198.3/140.6	168.2/146.8
70%	MSE/IEF	**108.5/150.9**	399.4/112.6	362.2/120.7	296.3/125.3	253.3/128.9	234.8/132.1	201.3/140.0

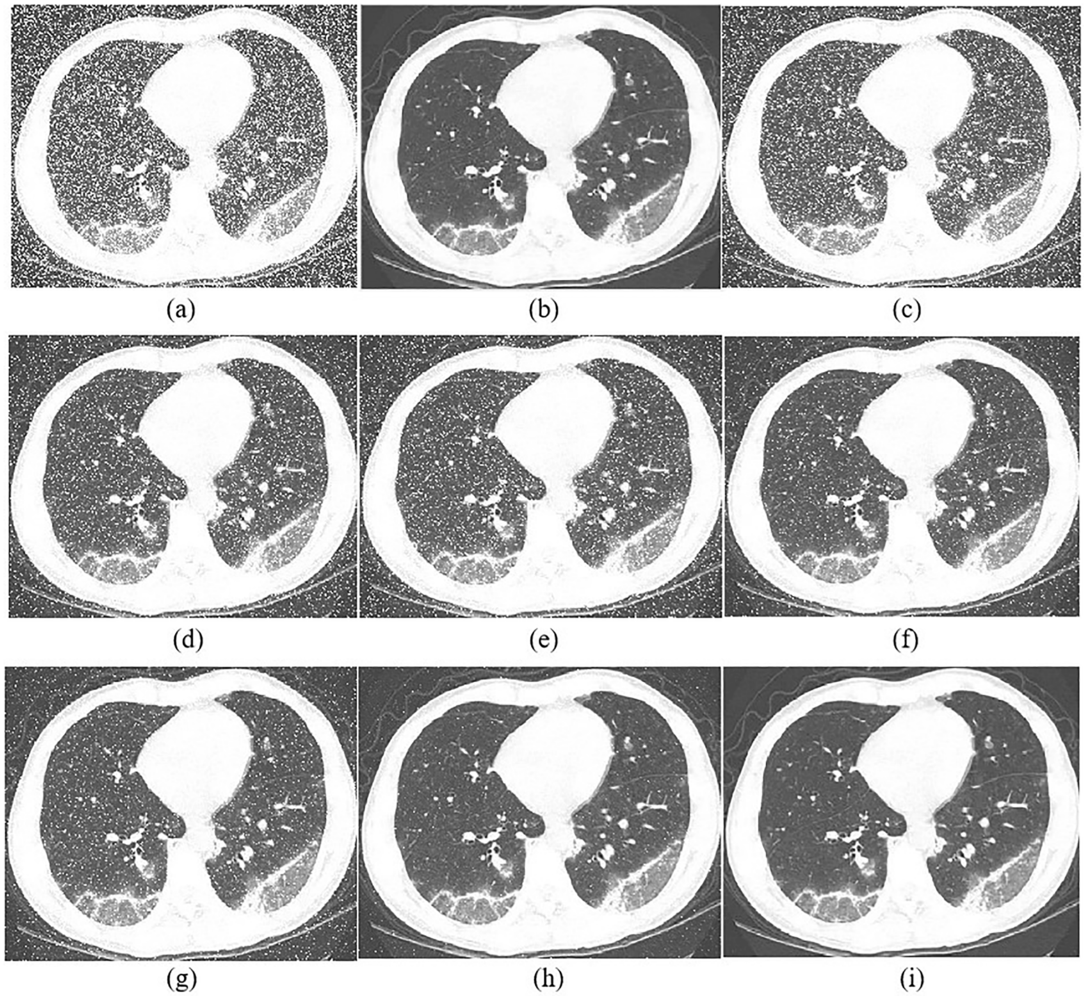

Fig. 10. CT image of adenovirus pneumonia (suspected cases of COVID-19) (a) impulse (40%) noise; (b) original CT image; (c) denoised image by TDMF; (d) denoised image by MMF; (e) denoised image by SMF; (f) denoised image by DBACMF; (g) denoised image by CWMF; (h) denoised image by AMF; (i) denoised image by TWMF.

Table 3
Comparison of TWMF with different methods for CT image of adenovirus pneumonia

Denoising method	MSE/dB	PSNR/dB	IEF
TDMF	289.7	23.5	131.2
MMF	247.8	24.2	137.5
SMF	198.2	25.2	142.6
DBACMF	156.9	26.2	149.9
CWMF	145.0	26.5	148.1
AMF	123.3	27.2	151.7
TWMF	**83.6**	**28.9**	**172.5**

f(i,j). If $\overline{f}_{max}$-T_0<f(i,j)<$\overline{f}_{max}$ or $\overline{f}_{min}$<f(i,j)<$\overline{f}_{min}$+T_0, this point may be a noise point, and skip to step 2. Step 2: calculate the average gray value f_{ave} of all pixels in the filter window. Step 3: set the second threshold T_1, if $|f(i,j) - f_{ave}|$-T_1>0, replace the weighted median value with the current point and repeat the above steps. The algorithm flow chart is shown in Fig.4.

3. Parameters optimization of weighted median filter based on adaptive hybrid genetic algorithm

The principle of the adaptive hybrid genetic optimization is as following: (i) Initializing the search space of $X_i(\alpha_1, \alpha_2)$, leading the genetic operators to search with $rmX_i = X_j + \varphi(\Delta x)$ to obtain the new solution $rmV_i(\alpha_1, \alpha_2)$; (ii) Using the parameter factors α_1 and α_2 to carry

Table 8
Comparison of TWMF with different methods for CT image of adenovirus pneumonia with different noise density

Noise	Index	TWMF	TDMF	MMF	SMF	DBACMF	CWMF	AMF
10%	MSE/IEF	**58.1/194.4**	124.5/148.8	117.4/150.7	108.5/53.8	100.7/159.8	96.4/164.7	88.2/168.4
20%	MSE/IEF	**65.4/186.7**	186.4/142.8	165.4/145.8	148.5/148.3	123.4/156.8	114.4/158.7	101.6/162.7
30%	MSE/IEF	**72.4/179.8**	226.5/137.9	211.8/141.5	176.8/44.6	144.6/151.5	129.5/153.8	116.4/156.9
40%	MSE/IEF	**83.6/172.5**	289.7/131.2	247.8/137.5	198.2/42.6	156.9/149.9	145.0/148.1	123.3/151.7
50%	MSE/IEF	**89.2/164.5**	321.6/125.4	277.5/132.6	221.5/37.6	178.5/141.6	179.5/144.3	138.6/148.7
60%	MSE/IEF	**97.4/158.7**	356.8/119.0	307.3/126.7	287.8/131.5	204.4/136.7	198.5/138.6	154.3/142.3
70%	MSE/IEF	**105.5/150.6**	388.6/116.4	344.5/121.9	324.4/125.3	236.4/131.7	226.8/135.3	178.6/137.7

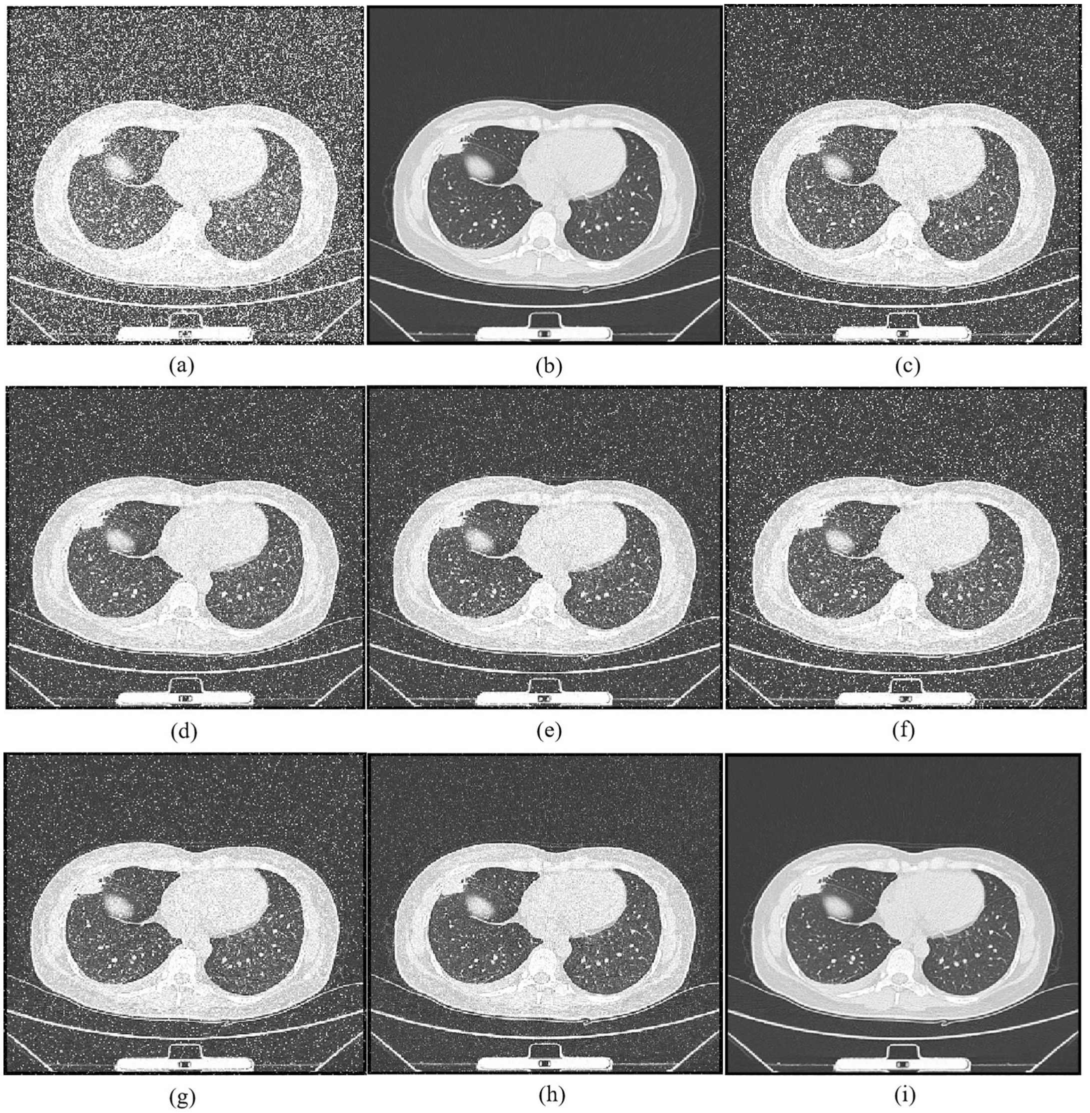

Fig. 11. CT image of early COVID-19 with non-symptom (a) impulse (40%) noise; (b) original CT image; (c) denoised image by TDMF; (d) denoised image by MMF; (e) denoised image by SMF; (f) denoised image by DBACMF; (g) denoised image by CWMF; (h) denoised image by AMF; (i) denoised image by TWMF.

Table 4
Comparison of TWMF with different methods for CT image of early COVID-19 with non-symptom

Denoising method	MSE/dB	PSNR/dB	IEF
TDMF	292.7	23.5	132.2
MMF	248.8	24.2	138.9
SMF	232.3	24.5	140.8
DBACMF	214.8	24.9	143.4
CWMF	178.5	25.6	146.7
AMF	149.2	26.4	149.6
TWMF	**92.8**	**28.5**	**179.2**

out the optimal weighted median filter; (iii) Calculating the value of PSNR as the fitness of the genetic algorithm; (iv) Using simulated annealing to cover the solution with high fitness over the low fitness as the current optimal solution. In this way, the cycle stops until the termination condition is established to obtain the optimal solution $rmX_k(\alpha_1, \alpha_2)$ corresponding to the highest fitness.

3.1. Improved operator strategy of adaptive hybrid genetic

In this paper, an adaptive hybrid genetic operator is proposed. In addition to retaining the "excellent" individuals in the parents to the next generation, individuals with close to average fitness in the parents should also be considered. If the fitness value of the offspring generation extracted in the "steady-state region" is higher than the average and close to the upper bound, it indicates that such parent individuals contain excellent gene patterns, it should be retained to the next generation. The diameter $D = f_{max} - f_{min}$ of the population is defined. The expression of the distance from the individual fitness value to the average value is $d = \left| f - f_{avg} \right|$. The neighborhood radius is defined as $\delta = \frac{D}{M}$(M is the population number). If the number of populations in the steady-state region is N, the density of populations in the steady-state region is $\rho = \frac{N}{M}$. We use the population density ρ to correct the crossover and mutation probability (Eqs. 19 and 20). The adaptive hybrid crossover probability can be expressed as:

Table 9
Comparison of TWMF with different methods for early COVID-19 with non-symptom by different noise density

Noise	Index	**TWMF**	TDMF	MMF	SMF	DBACMF	CWMF	AMF
10%	MSE/IEF	**72.1/200.4**	107.6/159.4	104.5/163.4	103.4/168.5	101.5/173.7	97.2/175.4	95.2/178.5
20%	MSE/IEF	**80.6/192.9**	164.7/150.4	155.7/152.8	157.4/160.8	156.4/161.6	121.5/162.6	112.3/165.5
30%	MSE/IEF	**85.5/185.4**	225.3/143.7	202.4/145.7	199.3/150.6	188.4/150.7	154.6/153.4	128.7/156.6
40%	MSE/IEF	**92.8/179.2**	292.7/132.2	248.8/138.9	232.3/140.8	214.8/143.4	178.5/146.7	149.2/149.6
50%	MSE/IEF	**98.3/172.7**	328.4/125.7	286.5/132.7	267.5/132.8	243.2/135.7	206.4/138.6	175.4/142.8
60%	MSE/IEF	**104.5/167.4**	376.4/118.6	312.4/125.6	301.3/125.7	288.9/128.4	235.3/132.7	202.5/136.6
70%	MSE/IEF	**112.7/159.4**	404.4/110.5	355.7/116.3	342.8/118.3	312.6/120.4	265.5/126.8	248.3/128.6

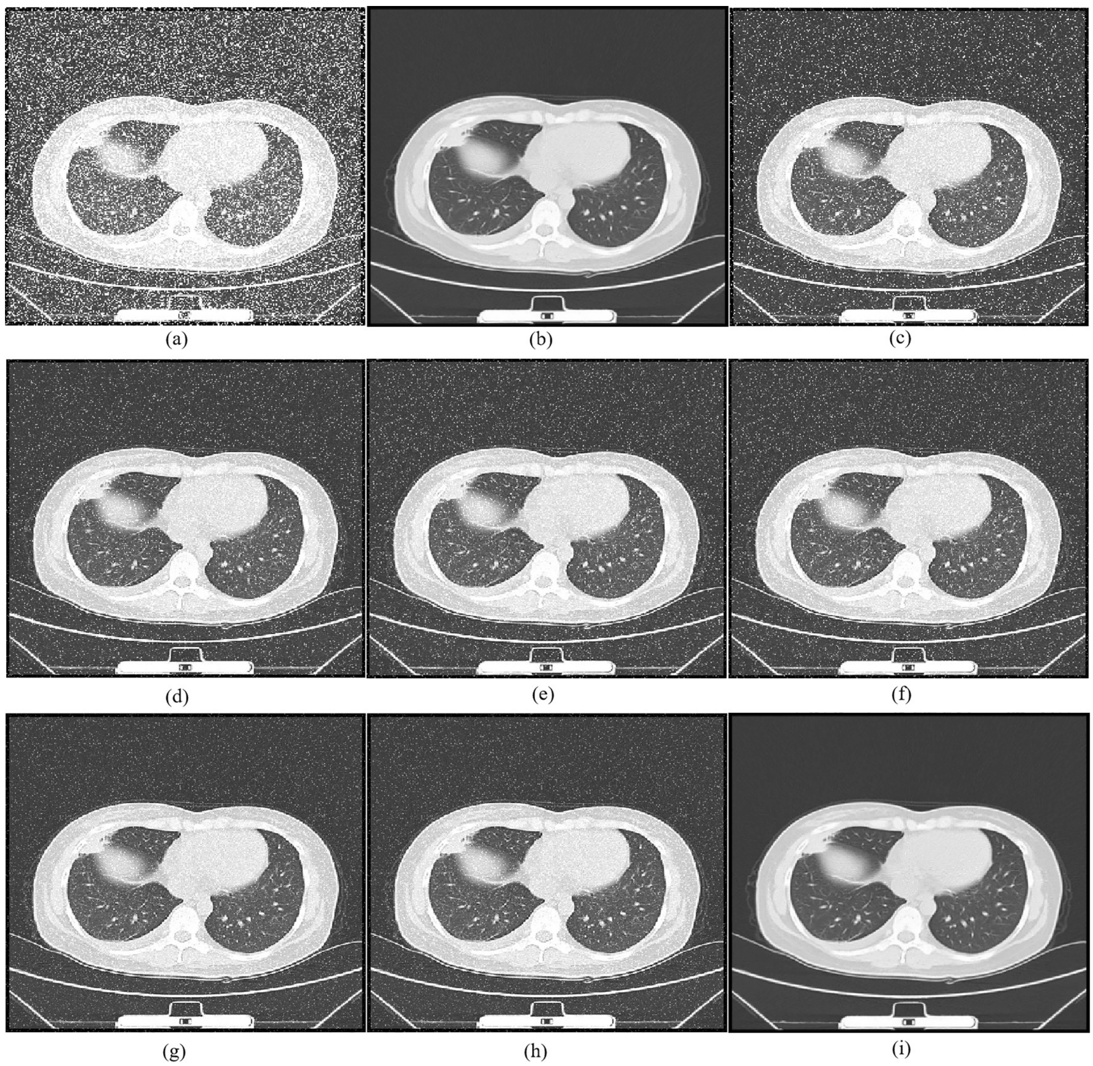

Fig. 12. CT image of advanced COVID-19 with non-symptom (a) impulse (40%) noise; (b) original CT image; (c) denoised image by TDMF; (d) denoised image by MMF; (e) denoised image by SMF; (f) denoised image by DBACMF; (g) denoised image by CWMF; (h) denoised image by AMF; (i) denoised image by TWMF.

Table 5
Comparison of TWMF with different methods for CT image of advanced COVID-19 with non-symptom.

Denoising method	MSE/dB	PSNR/dB	IEF
TDMF	285.7	23.6	121.6
MMF	261.7	24.0	129.4
SMF	233.3	25.1	137.7
DBACMF	196.5	25.2	142.1
CWMF	156.6	26.2	154.8
AMF	149.4	26.4	168.5
TWMF	**89.2**	**28.6**	**181.8**

Table 10
Comparison of TWMF with different methods for advanced COVID-19 with non-symptom by different noise density

Noise	Index	**TWMF**	TDMF	MMF	SMF	DBACMF	CWMF	AMF
10%	MSE/IEF	**60.1/207.3**	124.6/148.9	114.1/152.5	105.5/158.4	94.2/169.4	89.5/177.7	80.3/192.5
20%	MSE/IEF	**73.3/196.6**	187.4/138.5	175.3/143.7	168.2/150.6	150.5/158.9	126.9/168.4	113.2/185.6
30%	MSE/IEF	**82.6/188.8**	234.4/129.7	228.4/135.8	190.2/142.7	174.2/149.5	140.3/160.5	129.3/177.7
40%	MSE/IEF	**89.2/181.8**	285.7/121.6	261.7/129.4	233.3/137.7	196.5/142.1	156.6/154.8	149.4/168.5
50%	MSE/IEF	**96.4/172.8**	325.2/116.5	315.2/122.7	305.6/128.4	245.3/135.6	211.1/142.2	186.2/155.8
60%	MSE/IEF	**103.4/162.8**	359.7/112.3	345.5/117.9	327.7/122.2	288.3/129.7	256.5/133.8	215.1/143.4
70%	MSE/IEF	**114.3/150.1**	398.6/108.8	382.2/112.4	366.5/118.9	334.7/124.1	298.4/128.2	264.2/135.0

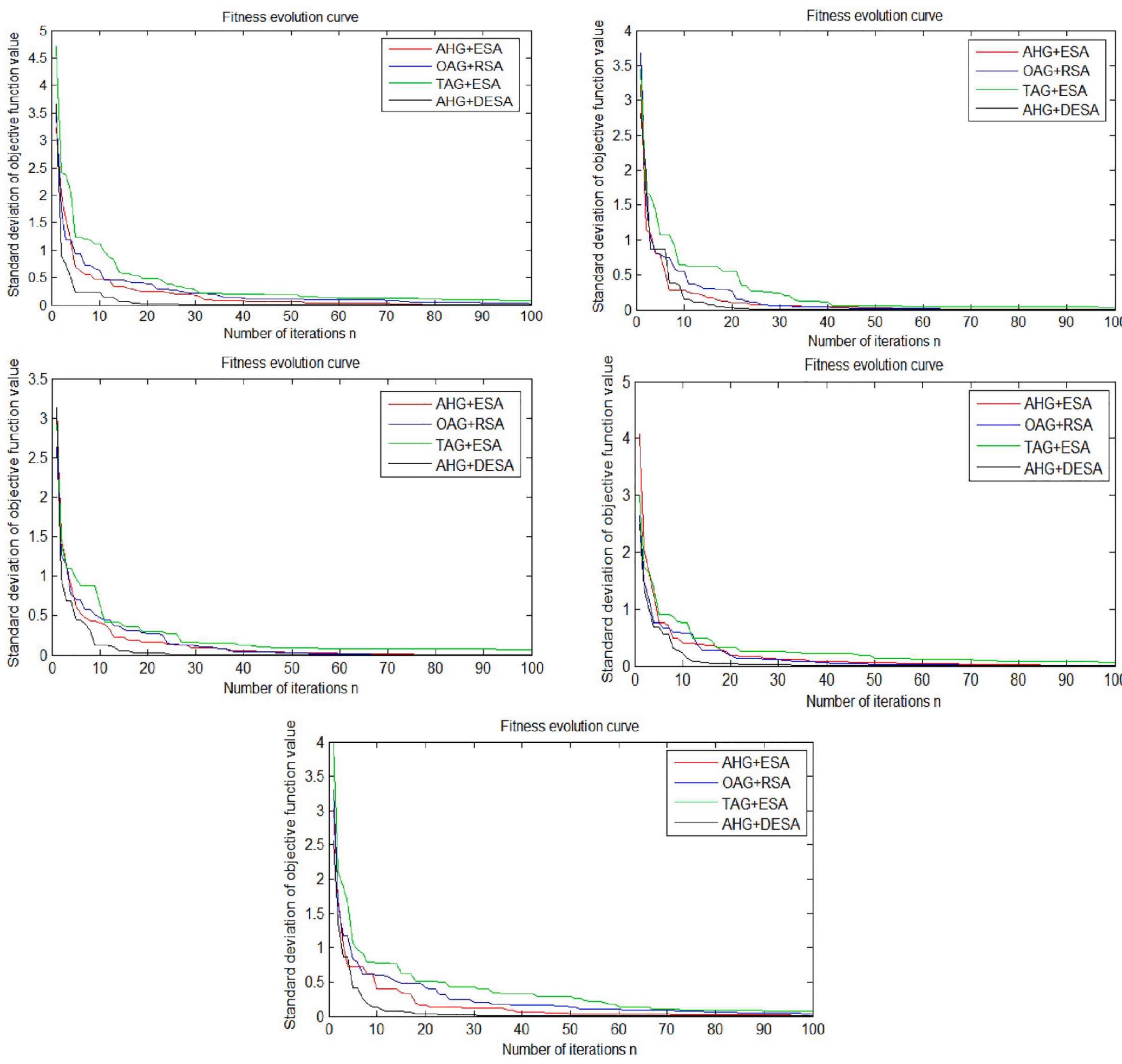

Fig. 14. Fitness evolution curve of denoising parameters optimization for different CT images. (a) CT image of early COVID-19; (b) CT image of advanced COVID-19; (c) CT image with non-symptom of early COVID-19; (d) CT image with non-symptom of advanced COVID-19; (d) CT image of adenovirus pneumonia.

$$P_c = \begin{cases} \rho \dfrac{k_1 \left(f_{max} - f^{/}\right)}{f_{max} - f_{avg}}, f^{/} \geqslant f_{avg}, \rho \leqslant \delta \\ \left(1 - \rho\right) \dfrac{k_1 \left(f_{max} - f^{/}\right)}{f_{max} - f_{avg}}, f^{/} \geqslant f_{avg}, \rho > \delta \\ \rho k_2, f^{/} < f_{avg}, \rho \leqslant \delta \\ \left(1 - \rho\right) k_2, f^{/} < f_{avg}, \rho > \delta \end{cases} \tag{15}$$

The adaptive hybrid mutation probability can be expressed as:

$$P_m = \begin{cases} \sqrt[l]{\dfrac{1}{n}} \rho, & \rho \leqslant \delta \\ \left(1 - \rho\right) \sqrt{l \dfrac{1}{n}}, & \rho > \delta \end{cases} \tag{16}$$

k_1 and k_2 are coefficients and $k_1, k_1 \leqslant 1$.The adaptive hybrid cross operation is shown in Fig.5, the adaptive hybrid mutation operation is shown in Fig.6.

Table 11
Time processing of CT image denoised under different methods

CT image	AHG + ESA	OAG + RSA	TAG + ESA	**AHG + DESA**
Early COVID-19	3.46	3.52	4.76	**2.66**
Advanced COVID-19	3.78	3.82	4.91	**2.83**
Non-symptom of early COVID-19	3.71	3.76	4.88	**2.81**
Non-symptom of advanced COVID-19	3.79	3.86	4.96	**2.87**
Adenovirus pneumonia	3.90	3.94	5.03	**2.97**

3.2. Improved simulated annealing algorithm

Derek [35] proposed metropolis simulated annealing algorithm criterion. This paper further improves the cooling function and designs an expression similar to the doppler effect temperature decline curve:

$$T = T_2\alpha^k\left(\cos\left(\pi/\left(2\left(1-k/K\right)\right)\right)\right) + \cos(\pi/(2T_0(1-k/K))) \tag{17}$$

The traditional exponential simulated annealing is difficult to reach the low temperature state when the number of iterations is small; the rapid simulated annealing drops to the low temperature state prematurely, making the subsequent iterative solution unchanged. The ”doppler” curve takes the advantages of the two algorithms and eliminates their defects. It not only tends to the low temperature unurgency, but also

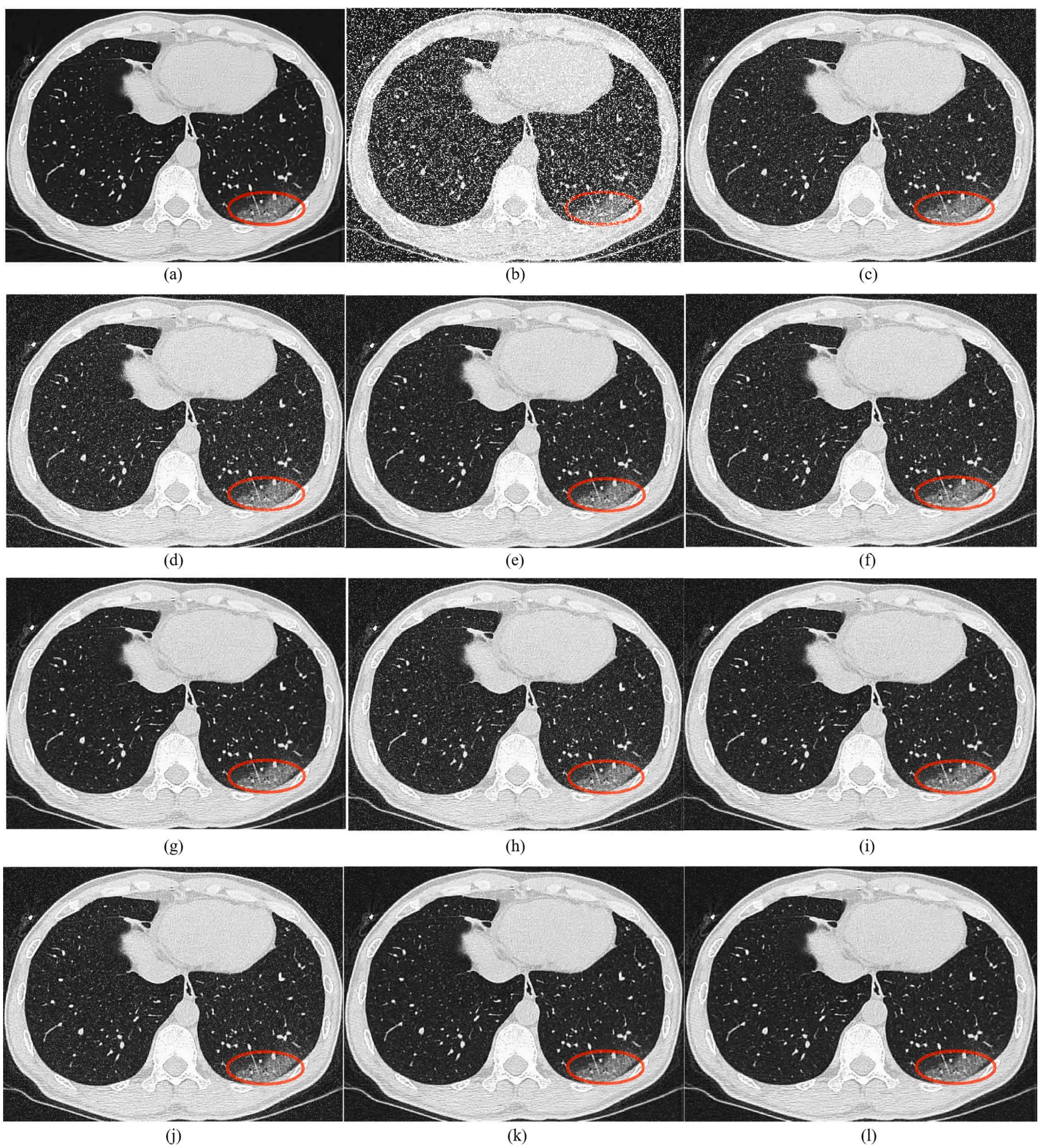

Fig. 15. CT image of early COVID-19 (a) original CT image; (b) impulse (40%) noise; (c) denoised image by TWSC; (d) denoised image by KSVD; (e) denoised image by ATIF; (f) denoised image by WNNM; (g) denoised image by BM3D; (h) denoised image by SAINT; (i) denoised image by DAAM; (j) denoised image by TNRD; (k) denoised image by DnCNN; (l) denoised image by TWMF.

Table 12
Comparison of TWMF with denoising SOTA methods for CT image of early COVID-19

Denoising method	MSE/dB	PSNR/dB	IEF
TWSC	108.5	27.8	152.5
KSVD	106.5	27.8	154.7
ATIF	103.3	27.9	156.3
WNNM	100.8	27.9	158.8
BM3D	98.3	28.0	160.2
SAINT	97.8	28.0	162.5
DAAM	96.2	28.1	163.0
TNRD	95.9	28.2	164.4
DnCNN	94.2	28.3	165.1
TWMF	**81.6**	**29.0**	**173.7**

continuously "tempering and heating up" in the second half of annealing, so that the algorithm has multiple opportunities to jump out of the local optimum during the optimization process, making it easier to find out the global optimal solution. K is the total number of iterations, and k is the current number of iterations. The flow chart of the adaptive hybrid genetic combined with the doppler effect simulated annealing algorithm is shown in Fig.7.

4. Experimental results

4.1. Parameters setting

Aiming at the different kinds of COVID-19 CT images including early COVID-19, advanced COVID-19, early COVID-19 with non-symptom, advanced COVID-19 with non-symptom, adenovirus pneumonia added into the density 40% of the impulse noise are tested by the Intel E8200 CPU 2.5 GHz, RAM 8G, Matlab 2016a.Two dimensional median filter (TDMF) [36], multiple median filter (MMF) [37], switching median filter (SMF) [38], discriminant-based asymmetric cropping median filter (DBACMF) [39], center weighted median filter (CWMF) [40], adaptive median filter (AMF) [15], adaptive threshold and optimized weighted median filter (paper method, TWMF) are used for simulation comparison tests. Then, impulse noise with different density (10%,20%,30%,40%,50%,60%,70%) is selected to add noise in the tested images, and finally the above methods are used for simulation tests in turn. The experimental parameters are set as: $k_1 = 0.6, k_2 = 0.7, T_2 = 150, \alpha = 0.8$, K = 100, M = 200.

4.2. Evaluation indexs

In order to objectively test the denoising effect of each method, mean square error (MSE), peak signal-to-noise ratio (PSNR) and image enhancement factor (IEF) are used to calculate the denoised image. The lower the MSE, the better the denoised image quality; the higher the peak signal-to-noise ratio and image enhancement factor, the better the denoising effect. The expression of MSE is:

$$MSE = \frac{1}{M \times N} \sum_{i=1}^{M} \sum_{j=1}^{N} [f(i,j) - \widehat{f}(i,j)]^2 \tag{18}$$

The expression of PSNR is:

$$PSNR = 10 \times \lg\left(\frac{255^2}{MSE}\right) \tag{19}$$

The expression of IEF is:

$$IEF = \frac{\sum_{i=1}^{M} \sum_{j=1}^{N} [x(i,j) - \widehat{f}(i,j)]^2}{\sum_{i=1}^{M} \sum_{j=1}^{N} [f(i,j) - \widehat{f}(i,j)]^2} \tag{20}$$

f(i,j) represents the denoised pixel, $\widehat{f}(i,j)$ represents the input pixel with impulse noise, x(i,j) represents the original pixel, M and N represents the length and width of the image respectively, the picture size is 512*512.

4.3. Denoising simulation experiments

Using the paper method and the comparison methods to do denoising simulations on the CT image of early COVID-19, and further comparing and analyzing the MSE, PSNR and IEF under different denoising methods. The comparative CT image denoising simulations of early COVID-19 are shown in Fig.8. The evaluation index values are shown in Table 1.

From the change trend of the data in the Table 1, compared with the comparative denoising methods, TWMF has increased the value of PSNR by about 5.5 dB, the value of MSE has been greatly reduced, the value of IEF has been increased by about 42 dB. It can be seen that the denoising effect for the CT image of early COVID-19 under TWMF is the best. There is no obvious change in the CT image of early COVID-19, the number of the lesion is small and the density is low. The traditional CT image denoising algorithms have the higher value of MSE and the lower value of IEF. It is easy to cause the CT image of early COVID-19 to be confused with noise, and it is easy to cause mistake diagnosis for patients with early COVID-19. The TWMF method improves the denoising accuracy for the CT image of early COVID-19. The CT image of early COVID-19 is simulated by denoising tests with different density (10%–70%) of impulse noise. The comparison for the MSE and IEF among different denoising methods by different density of the impulse noise is shown in Fig.13(a)(b). The evaluation index values are shown in Table 6.

When the value of MSE is smaller and the value of IEF is larger, it means that the denoised image is closer to the original image. It can be seen from the Fig.13(a)(b) that with the increase of the impulse noisy density, the PSNR is gradually reduced and the MES is gradually increased under different denoising methods. Compared with the different traditional denoising methods, the IEF of TWMF is still the largest, and the MSE of TWMF is still the smallest. In conclusion, compared with the traditional denoising methods, the improved median filter denoising algorithm in this paper increases the IEF and reduces the MSE for CT image of early COVID-19 to a certain extent with different noise density. It significantly improves the denoised effect. Using the TWMF and the comparison methods to do denoising simulations on the CT image of advanced COVID-19. The comparative CT image denoising simulations of advanced COVID-19 are shown in Fig.9. The evaluation index values are shown in Table 2.

From the change trend of the data in the Table 2, compared with the comparative denoising methods, TWMF has increased the value of PSNR by about 5.7 dB, the value of MSE has been greatly reduced, the value of IEF has been increased by about 45 dB. It can be seen that the denoising effect for the CT image of advanced COVID-19 under TWMF is best. The advanced stage of COVID-19 is characterized by increased number of lesions and increased density. The TWMF method improves the denoising accuracy for the CT image of advanced COVID-19 and it reduces the misdiagnosis rate for the advanced lesions. The CT image of advanced COVID-19 is simulated by denoising tests with different density(10%–70%) of impulse noise. The comparison for the MSE and IEF among different denoising methods with different density of the impulse noise is shown in Fig.13(c)(d).The evaluation index values are shown in Table 7.

It can be seen from the Fig.13(c)(d) and Table 7 that with the increase of the impulse noisy density, the IEF is gradually reduced and the MES is gradually increased under different denoising methods. Compared with the different traditional denoising methods, the IEF of TWMF is still the largest, and the MSE of TWMF is still the smallest. In conclusion, the TWMF significantly improves the denoised effect for CT image of advanced COVID-19 to a certain extent with different noisy density. Using the TWMF and the comparison methods to do denoising simulations on the CT image of adenovirus pneumonia (suspected cases of COVID-19). The comparative CT image denoising simulations of adenovirus pneumonia are shown in Fig.10. The evaluation index values are shown in Table 3.

From the change trend of the data in the Table 3, compared with the comparative denoising methods, TWMF has increased the value of PSNR by about 5.4 dB, the value of MSE has been greatly reduced, the value of IEF has been increased by about 41 dB. It can be seen that the denoising effect for the CT image of adenovirus pneumonia under TWMF is the best. The CT image of adenovirus pneumonia is patchy, small nodular ground-glass shadow, and then developing into consolidation shadow, bronchial wall thickening, visible mesh or strip shadow. The TWMF improves the denoising accuracy for the CT image of adenovirus pneumonia and reduces the misdiagnosis rate for the lesions. The CT image of adenovirus pneumonia are simulated by denoising tests with different density (10%–70%) of impulse noise. The comparison for the MSE and IEF among different methods with different density of the impulse noise is shown in Fig.13(e)(f). The evaluation index values are shown in Table 8.

It can be seen from the Fig.13(e)(f) and Table 8 that with the increase of the impulse noisy density, the IEF is gradually reduced and the MES is gradually increased under different denoising methods. Compared with the different traditional denoising methods, the IEF of TWMF is still the largest, and the MSE of TWMF is still the smallest. In conclusion, the TWMF method significantly improves the denoised effect for CT image of adenovirus pneumonia to a certain extent with different noisy density. Using the TWMF and the comparison methods to do denoising simulations on the CT image with non-symptom of early COVID-19. The comparative CT image denoising simulations are shown in Fig.11. The evaluation index values are shown in Table 4.

From the change trend of the data in the Table 4, compared with the comparative denoising methods, TWMF has increased the value of PSNR by about 5 dB, the value of MSE has been greatly reduced, the value of IEF has been increased by about 47 dB. It can be seen that the denoising effect for the CT image of early COVID-19 with non-symptom under TWMF is the best. The CT image of early COVID-19 with non-symptom are simulated by denoising test with different density (10%–70%) of impulse noise. The comparison for the MSE and IEF among different denoising methods with different density of the impulse noise is shown in Fig.13(g)(h). The evaluation index values are shown in Table 9.

It can be seen from the Fig.13(g)(h) and Table 9 that with the increase of the impulse noisy density, the IEF is gradually reduced and the MES is gradually increased under different denoising methods. Compared with the different traditional denoising methods, the IEF of TWMF is still the largest, and the MSE of TWMF is still the smallest. In conclusion, the TWMF significantly improves the denoised effect for CT image of early COVID-19 with non-symptom to a certain extent by different noisy density. Using the TWMF and the comparison methods to do denoising simulations on the CT image of advanced COVID-19 with non-symptom. The comparative CT image denoising simulations of advanced COVID-19 with non-symptom are shown in Fig.12. The evaluation index values are shown in Table 5.

From the change trend of the data in the Table 5, compared with the comparative denoising methods, TWMF has increased the value of PSNR by about 5.0 dB, the value of MSE has been greatly reduced, the value of IEF has been increased by about 60 dB. It can be seen that the denoising effect for the CT image of advanced COVID-19 with non-symptom under TWMF is the best. The CT image of advanced COVID-19 with non-symptom is simulated by denoising test with different density (10%–70%) of impulse noise. The comparison for the MSE and IEF among different denoising methods with different density of the impulse noise is shown in Fig.13(i)(j).The evaluation index values are shown in Table 10.

It can be seen from the Fig.13(i)(j) and Table 10 that with the increase of the impulse noisy density, the IEF is gradually reduced and the MES is gradually increased under different denoising methods. Compared with the different traditional denoising methods, the IEF of TWMF is still the largest, and the MSE of TWMF is still the smallest. In conclusion, the paper method significantly improves the denoised effect for CT image of advanced COVID-19 with non-symptom to a certain extent by different noisy density. Aiming at the different kinds of COVID-19 CT imagesadaptive hybrid genetic combined with exponential simulated annealing [41] (AHG + ESA) orthogonal adaptive genetic [42] combined with rapid simulated annealing [43] (OAG + RSA) traditional adaptive genetic [44] combined with exponential simulated annealing (TAG + ESA) adaptive hybrid genetic combined with doppler effect simulated annealing (AHG + DESA, paper method) are used for simulation comparison tests of denoising parameters optimization. The fitness evolution curve for different COVID-19 CT images are shown in Fig.14. The evaluation index values of time processing under different methods are shown in Table 11.

It can be seen from the Fig.14 and Table 11 that with the increase of the number of iterations, the standard deviation of the objective function value is gradually reduced and the processing time is gradually increased under different parameters optimization methods. Compared with the different comparison methods, the number of iterations of “HG + DESA” is still the smallest, and the processing time of “AHG + DESA” is still the fastest. In conclusion, the paper method (AHG + DESA) significantly improves the denoised effect for different kinds of COVID-19 CT images of parameters optimization.

4.4. Comparison to state-of-the-art methods

We compared the TWMF with 9 state-of-the-art approaches including TWSC [45], KSVD [21], activity-tuned image filtering(ATIF) [19], WNNM [23], BM3D [22], SAINT [46], DAAM [47], TNRD [48], DnCNN [20] to do denoising simulations on the CT image of early COVID-19, and further comparing and analyzing the MSE, PSNR and IEF under different denoising methods. The comparative CT image denoising simulations of early COVID-19 are shown in Fig.15. The evaluation index values are shown in Table 12. From the change trend of the data in the Table 12, compared with the comparative denoising methods, TWMF has increased the value of PSNR by about 1.2 dB, the value of MSE has been reduced by about 27 dB, the value of IEF has been increased by about 21 dB. It can be seen that the denoising effect for the CT image of early COVID-19 under TWMF is the best. The early stage of COVID-19 is characterized by less number of lesions and less density. The TWMF method improves the denoising accuracy for the CT image of early COVID-19 and reduces the missed diagnosis for the early lesions.

5. Conclusion

In this paper, a median filtering method based on multi-level threshold and parameters optimization is proposed. In this method, the pixels in the horizontal and vertical directions of the pixels to be processed, the multi-level threshold for detecting impulse noise is selected by comprehensive estimation, because the threshold changes with the movement of the window, which reflects the adaptability of threshold selection. In this paper, the algorithm gives different weight values to each pixel according to the gray distance between the pixel and the central pixel and the spatial distance between the pixel and the noise point to filter out the noise. The adaptive hybrid genetic algorithm combined with the doppler effect simulated annealing algorithm is used to determine the weight value of the improved median filter. The simulation results show that this method has greater advantages in denoising ability than other filtering methods of the iteration and the processing time, and the performance of detail protection is also greatly improved.

CRediT authorship contribution statement

Shuli Guo: Conceptualization, Methodology. **Guowei Wang:**

Writing & original draft, Data curation, Software. **Lina Han:** Writing - review & editing. **Xiaowei Song:** Investigation. **Wentao Yang:** Validation.

Declaration of Competing Interest

The authors declare that they have no known competing financial interests or personal relationships that could have appeared to influence the work reported in this paper.

Acknowledgements

This research has been partially funded by National Key R&D Program of China (2017YFF0207400) and project supported by Beijing Municipal Science and Technology Commission-Beijing Natural Science Foundation (M21018) and Beijing Natural Science Foundation-haidian District Joint Fund for original innovation (L192064).

References

[1] Chenyao Lin, Jie Xiang, Mingzhe Yan, Hongze Li, Shuang Huang, Changxin Shen, Comparison of throat swabs and sputum specimens for viral nucleic acid detection in 52 cases of novel coronavirus (sars-cov-2)-infected pneumonia (covid-19), Clinical Chemistry and Laboratory Medicine (CCLM) 58 (2020) 1089–1094.
[2] Yafang Li, Lin Yao, Jiawei Li, Lei Chen, Yiyan Song, Zhifang Cai, Chunhua Yang, Stability issues of rt-pcr testing of sars-cov-2 for hospitalized patients clinically diagnosed with covid-19, J. Med. Virol. (2020).
[3] Ioanna Smyrlaki, Martin Ekman, Andrea Lentini, Nuno Rufino de Sousa, Natali Papanicolaou, Martin Vondráček, Johan Aarum, Hamzah Safari, Shaman Muradrasoli, Antonio Gigliotti Rothfuchs, Jan Albert, Björn Högberg, and Björn Reinius. Massive and rapid covid-19 testing is feasible by extraction-free sars-cov-2 rt-pcr. Nature Commun., 11, 2020.
[4] Rajab Mardani, Abbas Ahmadi Vasmehjani, Fatemeh Zali, Alireza Gholami, Seyed Dawood Mousavi Nasab, Hooman Kaghazian, Mehdi Kaviani, and Nayeb Ali Ahmadi. Laboratory parameters in detection of covid-19 patients with positive rt-pcr; a diagnostic accuracy study. Arch. Acad. Emergency Med., 8, 2020.
[5] Alireza Tahamtan, Abdollah Ardebili, Real-time rt-pcr in covid-19 detection: issues affecting the results, Expert Rev. Mol. Diagn. (2020) 1–2.
[6] Tao Ai, Zhenlu Yang, Hongyan Hou, Chenao Zhan, Chong Chen, Wenzhi Lv, Qian Tao, Ziyong Sun, Liming Xia, Correlation of chest ct and rt-pcr testing in coronavirus disease 2019 (covid-19) in china: A report of 1014 cases, Radiology (2020).
[7] Adam Bernheim, Xueyan Mei, Mingqian Huang, Yang Yang, Zahi A. Fayad, Ning Zhang, Kaiyue Diao, Bin Lin, Xiqi Zhu, Kunwei Li, Shaolin Li, Hong Shan, Adam Jacobi, and Michael S Chung. Chest ct findings in coronavirus disease-19 (covid-19): Relationship to duration of infection. Radiology, 2020.
[8] Wei Xia, Yu. Jianbo Shao, Xue-Hua Peng Guo, Zhen Li, Hu. Daoyu, Clinical and ct features in pediatric patients with covid-19 infection: Different points from adults, Pediatr. Pulmonol. 55 (2020) 1169–1174.
[9] Yu. Xiang, Shuihua Wang, Yudong Zhang, Cgnet: A graph-knowledge embedded convolutional neural network for detection of pneumonia, Inform. Process. Manage. 58 (2021), 102411.
[10] Xin Zhang, Lu. Siyuan, Shuihua Wang, Yu. Xiang, Sujing Wang, Lun Yao, Yi Pan, Yudong Zhang, Diagnosis of covid-19 pneumonia via a novel deep learning architecture, J. Comput. Sci. Technol. (2021).
[11] Yan Li, Liming Xia, Coronavirus disease 2019 (covid-19): Role of chest ct in diagnosis and management, AJR (2020) 1–7.
[12] Lin Li, Lixin Qin, Xu. Zeguo, Youbing Yin, Xin Wang, Bin Kong, Junjie Bai, Lu. Yi, Zhenghan Fang, Qi Song, Kunlin Cao, Daliang Liu, Guisheng Wang, Xu. Qizhong, Xisheng Fang, Shiqin Zhang, Juan Xia, Jun Xia, Using artificial intelligence to detect covid-19 and community-acquired pneumonia based on pulmonary ct: Evaluation of the diagnostic accuracy, Radiology 296 (2020), 200905.
[13] Shuihua Wang, Xin Zhang, Yudong Zhang, Dssae: Deep stacked sparse autoencoder analytical model for covid-19 diagnosis by fractional fourier entropy, Mathematics 13 (2022) 1–20.
[14] Yu-Dong Zhang, Muhammad Attique Khan, Ziquan Zhu, Shuihua Wang, Pseudo zernike moment and deep stacked sparse autoencoder for covid-19 diagnosis, Comput., Mater. Continua 69 (2021) 3145–3162.
[15] Kesari Verma, Bikesh Kumar Singh, A.S. Thoke, An enhancement in adaptive median filter for edge preservation, Procedia Comput. Sci. 48 (2015) 29–36.
[16] C. Jaspin Jeba Sheela, G. Suganthi, An efficient denoising of impulse noise from mri using adaptive switching modified decision based unsymmetric trimmed median filter. Biomed. Signal Process. Control. 55, 2020.
[17] Vikas Gupta, Vijayshri Chaurasia, Madhu Shandilya, Random-valued impulse noise removal using adaptive dual threshold median filter, J. Vis. Commun. Image Represent 26 (2015) 296–304.
[18] Sajjad Ahmed, Saiful Islam, Median filter detection through streak area analysis, Digit. Invest. 26 (2018) 100–106.
[19] Lijun Zhao, Jie Liang, Huihui Bai, Lili Meng, Anhong Wang, Yao Zhao, Local activity-tuned image filtering for noise removal and image smoothing. ArXiv, abs/1707.02637, 2017.
[20] K. Zhang, Wangmeng Zuo, Yunjin Chen, Deyu Meng, Lei Zhang, Beyond a gaussian denoiser: Residual learning of deep cnn for image denoising. IEEE Trans. Image Process., 26:3142–3155, 2017.
[21] Chun Man Yan, Di Zhang, Youfei Hao, Jiahui Chen, An improved k-svd algorithm and its application for image denoising. In ICNC-FSKD, 2019.
[22] Ali Abdullah Yahya, Jieqing Tan, Benyue Su, Min Hu, Yibin Wang, Kui Liu, Ali Naser Hadi, Bm3d image denoising algorithm based on an adaptive filtering, Multimedia Tools Appl., 2020, pp. 1–37.
[23] Gu. Shuhang, Lei Zhang, Wangmeng Zuo, Xiangchu Feng, Weighted nuclear norm minimization with application to image denoising, in: 2014 IEEE Conference on Computer Vision and Pattern Recognition, 2014, pp. 2862–2869.
[24] Ou. Yang, Jianqiao Luo, Bailin Li, M.N. Shanmukha Swamy, Gray-level image denoising with an improved weighted sparse coding, J. Vis. Commun. Image Represent. 72 (2020), 102895.
[25] Dang Ngoc Hoang Thanh, Le Thi Thanh, Nguyen Ngoc Hien, Surya Prasath, Adaptive total variation l1 regularization for salt and pepper image denoising. Optik, 208:163677, 2020.
[26] Tran Dang Khoa Phan, A weighted total variation based image denoising model using mean curvature, Optik 217 (2020), 164940.
[27] Hongyao Deng, Jinsong Tao, Xiuli Song, Chunyuan Zhang, Estimation of the parameters of a weighted nuclear norm model and its application in image denoising, Inf. Sci. 528 (2020) 246–264.
[28] Youngjin Lee, Performance evaluation of noise reduction algorithm with median filter using improved thresholding method in pixelated semiconductor gamma camera system: a numerical simulation study. Nuclear, Eng. Technol. (2019).
[29] Elizabeth B. Herbst, Alexander L. Klibanov, John A. Hossack, F. William Mauldin, Dynamic filtering of adherent and non-adherent microbubble signals using singular value thresholding and normalized singular spectrum area techniques, in: Ultrasound in medicine & biology, 2021.
[30] Muhammad Habib, Ayyaz Hussain, Tae-Sun Choi, Adaptive threshold based fuzzy directional filter design using background information, Appl. Soft Comput. 29 (2015) 471–478.
[31] Ma.dhu.S. Nair, P.M. Ameera Mol, Direction based adaptive weighted switching median filter for removing high density impulse noise, Comput. Electr. Eng. 39 (2013) 663–689.
[32] Lu. Ching-Ta, Tzu-Chun Chou, Denoising of salt-and-pepper noise corrupted image using modified directional-weighted-median filter, Pattern Recognit. Lett. 33 (2012) 1287–1295.
[33] Zuoyong Li, Guanghai Liu, Xu. Yong, Yong Cheng, Modified directional weighted filter for removal of salt & pepper noise, Pattern Recognit. Lett. 40 (2014) 113–120.
[34] Tzu-Chao Lin, Chao Lin, Mu-Kun Liu, Chien-Ting Yeh, Partition-based fuzzy median filter based on adaptive resonance theory, Comput. Stand. Interfaces 36 (2014) 631–640.
[35] Derek M. Shore, Dow P. Hurst, Diane L. Lynch, Patricia H. Reggio, Identification of an endogenous allosteric modulator's binding site at the human cannabinoid-1 receptor, using forced-biased metropolis monte carlo simulated annealing method (mmc) and molecular dynamics, Biophys. J. 108 (2015).
[36] Yongkui Sun, Wen Tan, Tongwen Chen, A method to remove chattering alarms using median filters, ISA Trans. 73 (2018) 201–207.
[37] Aswini Kumar Samantaray, Priyanka Mallick, Decision based adaptive neighborhood median filter, Procedia Comput. Sci. 48 (2015) 222–227.
[38] Zhe Zhang, Deqiang Han, Jean Dezert, Yi Yang, A new adaptive switching median filter for impulse noise reduction with pre-detection based on evidential reasoning, Signal Process. 147 (2018) 173–189.
[39] Yakun Niu, Yao Zhao, Rongrong Ni, Robust median filtering detection based on local difference descriptor, Signal Process. Image Commun. 53 (2017) 65–72.
[40] Fazle Sadi, Soo Yeol Lee, Md. Kamrul Hasan, Removal of ring artifacts in computed tomographic imaging using iterative center weighted median filter, Comput. Biol. Med. 40 (1) (2010) 109–118.
[41] János Tóth, Henrietta Tomán, András Hajdu, Efficient sampling-based energy function evaluation for ensemble optimization using simulated annealing, Pattern Recognit. 107 (2020), 107510.
[42] Ihsan Erozan, Enes Çalişkan, A multi-objective genetic algorithm for a special type of 2d orthogonal packing problems, Appl. Math. Model. 77 (2020) 66–81.
[43] Alexander Kerr, Kieran J. Mullen, A comparison of genetic algorithms and simulated annealing in maximizing the thermal conductance of harmonic lattices, Comput. Mater. Sci. (2019).
[44] James C. Chen, Tzu-Li Chen, Ou. Ting-Chieh, Yu-Hsin Lee, Adaptive genetic algorithm for parcel hub scheduling problem with shortcuts in closed-loop sortation system, Comput. Ind. Eng. 138 (2019).
[45] Jun Xu, Lei Zhang, David Dian Zhang, A trilateral weighted sparse coding scheme for real-world image denoising. ArXiv, abs/1807.04364, 2018.
[46] Weisheng Dong, Guangming Shi, Xin Li, Nonlocal image restoration with bilateral variance estimation: A low-rank approach, IEEE Trans. Image Process. 22 (2013) 700–711.
[47] Youngjung Kim, Hyungjoo Jung, Dongbo Min, Kwanghoon Sohn, Deeply aggregated alternating minimization for image restoration, in: 2017 IEEE Conference on Computer Vision and Pattern Recognition (CVPR), 2017, pp. 284–292.
[48] Yunjin Chen, Thomas Pock, Trainable nonlinear reaction diffusion: A flexible framework for fast and effective image restoration, IEEE Trans. Pattern Anal. Mach. Intell. 39 (2017) 1256–1272.